Concentration Profiles near an Activated Enzyme

Soohyung Park and Noam Agmon*

Institute of Chemistry and the Fritz Haber Research Center, The Hebrew University, Jerusalem 91904, Israel

Received: May 2, 2008; Revised Manuscript Received: June 25, 2008

When a resting enzyme is activated, substrate concentration profile evolves in its vicinity, ultimately tending to steady state. We use modern theories for many-body effects on diffusion-influenced reactions to derive approximate analytical expressions for the steady-state profile and the Laplace transform of the transient concentration profiles. These show excellent agreement with accurate many-particle Brownian-dynamics simulations for the Michaelis−Menten kinetics. The steady-state profile has a hyperbolic dependence on the distance of the substrate from the enzyme, albeit with a prefactor containing the complexity of the many-body effects. These are most conspicuous for the substrate concentration at the surface of the enzyme. It shows an interesting transition as a function of the enzyme turnover rate. When it is high, the contact concentration decays monotonically to steady state. However, for slow turnover it is nonmonotonic, showing a minimum due to reversible substrate binding, then a maximum due to diffusion of new substrate toward the enzyme, and finally decay to steady state. Under certain conditions one can obtain a good estimate for the critical value of the turnover rate constant at the transition.

I. Introduction

The Michaelis−Menten (MM) mechanism[1] is a widely applicable reaction scheme in biological processes. For enzymatic reactions, this mechanism has been routinely applied to the observed kinetics.[2−7] MM kinetics was found to be applicable even for single molecules, when the enzyme undergoes large conformational fluctuations.[8−10] The classical description of the MM kinetics ignores the many-body competition and diffusion effects. These effects may be important in biological systems, particularly inside the cell, when substrate diffusion is slowed down by microscopic obstacles even more than by viscosity.[11,12]

Modern theories of (many-body) diffusion-influenced reactions,[13−23] which are successful in treating such effects in reversible reactions,[24−28] have only recently been extended to the MM mechanism.[29−31] In a recent work,[31] we have shown that under general conditions the MM equation formally holds, albeit with a concentration-dependent Michaelis parameter, K_M. The nonconstancy of this enzymatic "constant" is significant when the ratio of the catalytic and diffusion constants (k_p/k_D) is large.

Yet the above-mentioned theoretical treatments have focused on the kinetics of product formation, whereas the spatio-temporal distribution of diffusing substrate molecules received little attention. For an irreversible reaction, the Smoluchowski theory provides analytic expressions for the concentration profile around a reactive trap.[32] Following activation of this trap, a concentration gradient spreads out by diffusion, approaching its ultimate steady-state (SS) profile monotonically. In contrast, for the reversible $A + B \rightleftarrows C$ (ABC) reaction, the concentration of diffusing particles around the reaction site first decreases and then restores its bulk value at long times.[24,33] The MM scheme involves two steps, the first of which is reversible and the second, product formation step (rate constant k_p), is irreversible. Thus both behaviors may be expected here.

The present work focuses on the time (t) evolution of the concentration profile of substrate molecules around an enzyme that becomes activated at $t = 0$. Utilizing the previously developed uniform theory[31] for the MM kinetics, we obtain an accurate theoretical description which is verified by Brownian dynamics (BD) simulations. We treat both the spatial and temporal dependence of the substrate concentration, from its initial uniform distribution and up to its final steady-state (SS) limit. A transition from monotonic to nonmonotonic approach to SS is observed as a function of k_p. It is explained quantitatively by the modern theories of diffusion-influenced reactions and qualitatively as competition between diffusion and enzymatic turnover, from which follows an approximate condition for observing nonmonotonic behavior.

II. Theoretical Background

The MM mechanism is described as follows. In its first step, a free enzyme (A) and a substrate molecule (B) can associate with the rate constant κ_1, to form an enzyme−substrate complex (C). Then, this complex may redissociate into the enzyme and its substrate with the rate constant κ_2, or proceed to the second step of product formation. In this step, the complex dissociates with the rate-constant k_p, into the product (P) and the original enzyme (A). (k_p is known as the "catalytic constant" or "turnover number".) The reaction scheme is thus

$$A + B \underset{\kappa_2}{\overset{\kappa_1}{\rightleftharpoons}} C \xrightarrow{k_p} A + P \tag{2.1}$$

We assume that reaction between enzyme and substrate occurs only upon collision, at the contact distance, R. Interactions between particles are ignored and the enzyme is assumed to be static, hence its diffusion constant vanishes ($D_A = 0$). This may not be a bad approximation for a large biological molecule. B and P diffuse with the corresponding diffusion constants D_B and D_P. However, P may be ignored because it is only a spectator in the reversible reaction.

* Corresponding author. Email: agmon@fh.huji.ac.il.

10.1021/jp803873p CCC: $40.75
Published on Web 08/29/2008

We consider the MM mechanism in the pseudounimolecular limit, when the bulk concentration of B is much larger than those of A and C. It can thus be regarded as a constant, b_0. The concentrations of A and C vary with time: [A](t) and [C](t), while that of B varies both with time and its distance, r, from A (or C): [B](r,t). As $r \to \infty$, [B](r,t) $\to b_0$. The normalized concentrations of A and C are defined as

$$a(t) \equiv [\mathrm{A}](t)/\{[\mathrm{A}](0) + [\mathrm{C}](0)\}$$

$$c(t) \equiv [C](t)/\{[\mathrm{A}](0) + [\mathrm{C}](0)\}$$

The normalized concentration profile of B is defined as $b(r,t) \equiv [\mathrm{B}](r,t)/b_0$. We consider a system with an initially free enzyme embedded in a uniform substrate concentration, i.e., $a(0) \equiv 1$, $c(0) \equiv 0$, and $b(r,0) \equiv 1$.

A. Kinetic Hierarchy. From the reaction diffusion equations for the many-body joint probability distribution functions,[34] one can obtain evolution equations for an infinite hierarchy of distribution functions.[13,14] These are obtained by integrating over all coordinates, all except one, two, etc. For the MM mechanism, the first two levels in the hierarchy can be written as

$$\frac{\mathrm{d}a(t)}{\mathrm{d}t} = -\frac{\mathrm{d}c(t)}{\mathrm{d}t} = -\kappa_1 \rho_{\mathrm{AB}}(R,t) + (\kappa_2 + k_\mathrm{p})c(t) \quad (2.2a)$$

$$\frac{\partial}{\partial t}\rho_{\mathrm{AB}}(r,t) = \mathscr{L}_r \rho_{\mathrm{AB}}(r,t) - [\kappa_1 \rho_{\mathrm{AB}}(R,t) - \kappa_2 c(t)]\frac{\delta(r-R)}{4\pi R^2} - \kappa_1 \rho_{\mathrm{ABB}}(r,R,t) + (\kappa_2 + k_\mathrm{p})\rho_{\mathrm{CB}}(r,t) \quad (2.2b)$$

$$\frac{\partial}{\partial t}\rho_{\mathrm{CB}}(r,t) = \mathscr{L}_r \rho_{\mathrm{CB}}(r,t) + \kappa_1 \rho_{\mathrm{ABB}}(r,R,t) - (\kappa_2 + k_\mathrm{p})\rho_{\mathrm{CB}}(r,t) \quad (2.2c)$$

where $\delta(x)$ is the Dirac delta function and $\mathscr{L}_r$ is the diffusion operator, which is defined as

$$\mathscr{L}_r \equiv \frac{D_\mathrm{B}}{r^2}\frac{\partial}{\partial r} r^2 \frac{\partial}{\partial r} \quad (2.3)$$

The diffusion constant in this operator is D_B, because we have assumed that A is static.

The AB pair distribution function, $\rho_{\mathrm{AB}}(r,t)$, is defined as $\rho_{\mathrm{AB}}(r,t) \equiv b_0 p_{\mathrm{AB}}(r,t)$, where $p_{\mathrm{AB}}(r,t)$ is the probability density of finding an AB pair separated by r at time t. In other words, $\rho_{\mathrm{AB}}(r,t)$ is the concentration of B around the free trap, A, at time t. Similarly, $\rho_{\mathrm{CB}}(r,t)$ is the concentration of B around the occupied trap, C, at time t. The three-particle distribution function, $\rho_{\mathrm{ABB}}(r,r',t)$, is similarly defined by $\rho_{\mathrm{ABB}}(r,r',t) \equiv b_0^2 p_{\mathrm{ABB}}(r,r',t)$, where $p_{\mathrm{ABB}}(r,r',t)$ is the joint probability density of finding two B particles at distances r and r' from A at t.

The lowest level in the hierarchy, eq 2.2a, describes the kinetics of $c(t)$. It is coupled to the second level via the reactive pair distribution, $\rho_{\mathrm{AB}}(R,t)$. The second level of the hierarchy, eqs 2.2b and 2.2c, depict the evolution of the reactive and unreactive pair distributions, $\rho_{\mathrm{AB}}(r,t)$ and $\rho_{\mathrm{CB}}(r,t)$, respectively. These couple to the third level via the triplet density, $\rho_{\mathrm{ABB}}(r,R,t)$. Since we are interested here in the concentration profile of B, $[\mathrm{B}](r,t) = \rho_{\mathrm{AB}}(r,t) + \rho_{\mathrm{CB}}(r,t)$, we need not go beyond the level of doublets.

Initially, the pair distribution functions are given by $\rho_{\mathrm{AB}}(r,0) = b_0$ and $\rho_{\mathrm{CB}}(r,0) = 0$. Because reactions are introduced by sink terms, it is assumed that these functions obey a reflecting boundary condition at $r = R$ (and also at $r = \infty$). Hence

$$\int_R^\infty d^3 r\, \mathscr{L}_r \rho_{\mathrm{AB}}(r,t) = \int_R^\infty d^3 r\, \mathscr{L}_r \rho_{\mathrm{CB}}(r,t) = 0$$

Spatial integration of $\rho_{\mathrm{AB}}(r,t)$ and $\rho_{\mathrm{CB}}(r,t)$ gives $b_0 a(t)$ and $b_0 c(t)$, respectively. Similarly, integration of $\rho_{\mathrm{ABB}}(r,r',t)$ over space with respect to r' (or r) gives $b_0 \rho_{\mathrm{AB}}(r,t)$ [or $b_0 \rho_{\mathrm{AB}}(r',t)$]. Thus eq 2.2a is obtained by integrating the higher level in the hierarchy, i.e., eqs 2.2b and 2.2c.

The infinite hierarchy in eqs 2.2 is intractable and does not admit an exact solution. Simple truncation of this hierarchy (e.g., by writing higher order distribution functions as products of lower-order ones) usually does not give good results, particularly for the long-time asymptotic behavior. Therefore, we discuss another starting point, that of a rate-kernel equation which is formally equivalent to the full hierarchy but more amenable to approximations.[14] However, we will return to the hierarchical equations when we discuss the concentration profile in section III.

B. Memory Kernel. The starting point of our previous work was the formally exact rate-kernel equation, which can be obtained from eqs 2.2:[14]

$$\frac{\mathrm{d}a(t)}{\mathrm{d}t} = -\frac{\mathrm{d}c(t)}{\mathrm{d}t} = -\kappa_1 b_0 \int_0^t \mathrm{d}t'\, \Sigma(t-t')a(t') + \kappa_2 \int_0^t \mathrm{d}t'\, \Sigma(t-t')c(t') + k_\mathrm{p} c(t) \quad (2.4)$$

where $\Sigma(t)$ is a memory kernel which accounts for the history of the repeated interactions in the reversible reaction. It may depend on the rate constants, substrate concentration, diffusion constant, and contact distance, but it is identical for both directions of the reversible reaction.

In Laplace space [$\hat{f}(s) \equiv \int_0^\infty \mathrm{d}t\, \mathrm{e}^{-st} f(t)$ for any function of time, $f(t)$], the convolutions in eq 2.4 become multiplications. Inserting the Laplace transform (LT) of eq 2.4 into that of eq 2.2a gives

$$s\hat{a}(s) - 1 = -s\hat{c}(s) \equiv \hat{\alpha}(s) + k_\mathrm{p}\hat{c}(s) = [-\kappa_1 b_0 \hat{a}(s) + \kappa_2 \hat{c}(s)]\hat{\Sigma}(s) + k_\mathrm{p}\hat{c}(s) \quad (2.5)$$

where $\hat{\alpha}(s)$ is the LT of

$$\alpha(t) \equiv -\kappa_1 \rho_{\mathrm{AB}}(R,t) + \kappa_2 c(t) \quad (2.6)$$

It can be interpreted as the net dissociation rate of the enzyme−substrate complex via the reversible bimolecular reaction, C $\rightleftarrows$ A + B.

By introducing the "diffusion factor function" (DFF), $\hat{F}(s) \equiv \hat{\Sigma}(s)^{-1}$, which contains the many-body diffusion effects, we rewrite eq 2.5 as

$$\hat{c}(s) = -\frac{\hat{\alpha}(s)}{s_\mathrm{p}} = \frac{\kappa_1 b_0}{s[s_\mathrm{p}\hat{F}(s) + \lambda_0]} \quad (2.7)$$

where $\lambda_0 \equiv \kappa_1 b_0 + \kappa_2$ and $s_\mathrm{p} \equiv s + k_\mathrm{p}$.

The above formal solution depends on the unknown function $\hat{F}(s)$. One may nevertheless show that the DFF has some general properties: (i) $F(0) \equiv \lim_{s\to\infty}\hat{F}(s) = 1$; (ii) $s\hat{F}(s) \to 0$ as $s \to 0$, so that $\hat{F}(0)$ is a finite number.[31] The behavior near $s = 0$ enables us to obtain the SS solution in terms of $\hat{F}(0)$. The SS concentration of the enzyme−substrate complex, c_{ss}, is obtained by taking the limit that $s\hat{c}(s) \to c_{\mathrm{ss}}$ as $s \to 0$. One finds that

$$c_{\mathrm{ss}} = b_0/(K_\mathrm{M} + b_0) \quad (2.8a)$$

$$K_\mathrm{M} \equiv [k_\mathrm{p}\hat{F}(0) + \kappa_2]/\kappa_1 \quad (2.8b)$$

The SS net dissociation rate of the enzyme−substrate complex via reversible bimolecular reaction can be obtained from eq 2.7 as

$$\alpha_{\mathrm{ss}} = \lim_{s\to 0} s\hat{\alpha}(s) = -k_\mathrm{p} c_{\mathrm{ss}} \quad (2.9)$$

Thus, the net reaction rate, $\alpha(t) + k_\mathrm{p}c(t)$, vanishes at SS.

C. Approximations for the Diffusion Factor Function. In order to obtain a tractable DFF, modern theories of diffusion-influenced bimolecular reactions[13−23] truncate the infinite hierarchy of eqs 2.2 by various approximations. The resulting DFFs in these approximations share the general structure:

$$\hat{F}(s) = 1 + \kappa_1[\mu g(s) + (1-\mu)g(s_p + \lambda)] \tag{2.10}$$

where

$$g(s) \equiv \hat{G}(R, s|R) = [k_D(1 + \sqrt{\tau s})]^{-1} \tag{2.11a}$$

$$\hat{G}(r, s|R) = g(s)e^{-\sqrt{\tau s}(r/R-1)}R/r \tag{2.11b}$$

Here $k_D \equiv 4\pi RD_B$ is the diffusion-controlled rate constant and $\tau \equiv R^2/D_B$ the diffusional time. The Green function, $\hat{G}(r,s|r_0)$, is the solution of the LT of the diffusion equation without any reaction terms:

$$(s - \mathscr{L}_r)\hat{G}(r, s|r_0) = \delta(r - r_0)/(4\pi r_0^2) \tag{2.12}$$

where $r, r_0 \geq R$. Reflecting boundary conditions (vanishing derivative) are imposed at $r = R$ and $r = \infty$.

The long-time behavior is determined by the behavior of the LT as $s \to 0$. In this limit one has

$$\hat{F}(0) = 1 + \frac{\kappa_1}{k_D}\frac{1 + \mu\sqrt{\tau(k_p + \lambda)}}{1 + \sqrt{\tau(k_p + \lambda)}} \tag{2.13}$$

The coefficient μ has the same general form:

$$\mu = (k_2 + k_p)/(\lambda + k_p) \tag{2.14}$$

in all various theories, except that the effective rate parameters, k_i ($i = 1, 2$), depend differently on the microscopic ones, κ_i. Note that, in analogy to the definition of λ_0 above, we have defined here $\lambda \equiv k_1 b_0 + k_2$.

The simplest multi-particle diffusion theory is the integral encounter theory (IET),[17] valid only in the low-concentration limit. Setting $b_0 \approx 0$, one has for the IET that $\mu = 1$. In the more elaborate approximations, μ depends on the κ_i and sometimes even on s. Thus, in the self-consistent relaxation time approximation (SCRTA),[18] k_i is specified by the self-consistent SS condition for the MM mechanism,[31] $k_i^{SC} \equiv \kappa_i/\hat{F}(0)$. For the multiparticle kernel theories (MPK),[14−16] these rate coefficients become time-dependent, $k_i = \hat{k}_i(s)$. Among these, it has been shown[15,16] that the MPK2 and MPK3 are equivalent to the renormalized kinetic theory (KT)[20,21] and the modified encounter theory (MET),[22,23] respectively. For the MPK3/MET,[16] the rate coefficients are calculated at every s from $\hat{k}_i(s) \equiv \kappa_i/[1 + \kappa_1 g(s)]$. For the MPK2/KT,[30] these are calculated self-consistently from $\hat{k}_i(s) \equiv \kappa_i/\hat{F}(s)$. For the Michaelis−Menten unified Smoluchowski approximation (MM-USA),[31] one adopts k_i^{SC} and further replaces[18] $g(s_p + \lambda)$ by $b_{eff}/[\hat{\mathscr{R}}(s_p;b_{eff})^{-1} - s_p] - 1/\kappa_1$, where $b_{eff} = b_0 + \kappa_2/\kappa_1$. $\hat{\mathscr{R}}(s;b_{eff})$ is the LT of the relaxation function, $\mathscr{R}(t;b_{eff}) = \exp[-b_{eff}\int_0^t dt'\, k_{irr}(t')]$, where the irreversible rate function is defined as $k_{irr}(t) \equiv \kappa_1 b(R,t)$ for $\kappa_2 = k_p = 0$.

Table 1 in ref 31 summarizes the functional form of $\hat{F}(0)$ in these various theoretical approximations. We compare them below with the simulated substrate concentration profiles.

III. Concentration Profile

As the reaction proceeds, a concentration gradient of B around the static enzyme develops. From the definitions of $\rho_{AB}(r,t)$ and $\rho_{CB}(r,t)$, it is clear that the time- and distance-dependent concentration of B is the sum of these pair distribution functions: $[B](r,t) = \rho_{AB}(r,t) + \rho_{CB}(r,t)$. Thus, by summing eqs 2.2b and 2.2c, one obtains the evolution equation for the concentration profile:

$$\frac{\partial}{\partial t}[B](r,t) = \mathscr{L}_r[B](r,t) + \alpha(t)\frac{\delta(r-R)}{4\pi R^2} \tag{3.1}$$

Note that the above equation is formally exact because it is obtained without any truncation from the exact infinite hierarchy. Of course, $\alpha(t)$ is unknown, and thus depends on approximations for the DFF.

With the initial condition $[B](r,0) = b_0$, one finds that the LT of the normalized concentration profile, $b(r,t) \equiv [B](r,t)/b_0$, obeys the following differential equation

$$(s - \mathscr{L}_r)\hat{b}(r,s) = 1 + \frac{\hat{\alpha}(s)}{b_0}\frac{\delta(r-R)}{4\pi R^2} \tag{3.2}$$

Operating on both sides with $(s - \mathscr{L}_r)^{-1}$ and inserting eq 2.12 gives

$$\hat{b}(r,s) = \frac{1}{s} + \frac{\hat{\alpha}(s)}{b_0}\hat{G}(r, s|R) \tag{3.3}$$

where $\hat{G}(r,s|R)$ is given by eq 2.11b

The SS solution of the above equation is obtained by taking the limit that $s\hat{b}(r,s) \to b_{ss}(r)$ as $s \to 0$, which is given by

$$1 - b_{ss}(r) = \frac{k_p/k_D}{K_M + b_0}\frac{R}{r} = \frac{k_p\kappa_1/k_D}{k_p\hat{F}(0) + \lambda_0}\frac{R}{r} \tag{3.4}$$

Thus the many-body effects enter explicitly even in the SS distribution, through the DFF $\hat{F}(0)$. Note that the SS concentration profile is, of course, a solution of the SS diffusion equation

$$\mathscr{L}_r[B]_{ss}(r) = k_p c_{ss}\frac{\delta(r-R)}{4\pi R^2} \tag{3.5}$$

This equation is isomorphic with a SS diffusion equation for an irreversible reaction,[32] with the effective irreversible rate coefficient $k_p c_{ss}$ obtained from the MM scheme at SS. A double spatial integration then leads to the solution in eq 3.4 with its familiar hyperbolic r-dependence.

Let us discuss in more detail the behavior of $b(r,t)$ at short and long times. Define the deviation of $b(r,t)$ from its initial value by $\Delta b(r,t) \equiv b(r,t) - 1$. Using eq 3.3, it can be written in Laplace space as

$$\Delta\hat{b}(r,s) = \Delta\hat{b}_{rev}(r,s) + \Delta\hat{b}_{irr}(r,s) \tag{3.6}$$

where we define its reversible and irreversible components by

$$\Delta\hat{b}_{rev}(r,s) \equiv -s\hat{c}(s)\hat{G}(r, s|R)/b_0 \tag{3.7a}$$

$$\Delta\hat{b}_{irr}(r,s) \equiv -k_p\hat{c}(s)\hat{G}(r, s|R)/b_0 \tag{3.7b}$$

The LT of the concentration profiles are thus proportional to the binding probability, $\hat{c}(s)$ in eq 2.7. In the time domain, these become a convolution of the dissociation process with free diffusion from contact to r.

We now show that $b(r,t)$ approaches $b_{rev}(r,t)$ at short times, when the reversible reaction (A + B ⇄ C) dominates. It approaches $b_{irr}(r,t)$ at long times, when irreversible product formation (C → A + P) dominates. At the initial stages of reaction ($s \to \infty$), $\Delta\hat{b}_{rev}(r,s) \gg \Delta\hat{b}_{irr}(r,s)$, therefore $\Delta\hat{b}(r,s) \approx \Delta\hat{b}_{rev}(r,s)$, where

$$\Delta\hat{b}_{\rm rev}(r,s) \approx -\frac{\kappa_1 \widehat{G}(r,s|R)}{s\widehat{F}(s)+\lambda_0+k_{\rm p}} \tag{3.8}$$

The denominator derives from $s_{\rm p}\hat{F}(s) \approx s\hat{F}(s) + k_{\rm p}$ at large s, when $\hat{F}(s) \to 1$. Note that the structure of eq 3.8 is the same as that for the ABC reaction with the dissociation rate constant being replaced by $\kappa_2 + k_{\rm p}$.[24] Therefore, $b(r,t)$ at short times resembles that for the reversible reaction.

Similarly, at long times ($s \to 0$), $\Delta\hat{b}(r,s) \approx \Delta\hat{b}_{\rm irr}(r,s)$ whose asymptotic behavior is

$$\Delta\hat{b}_{\rm irr}(r,s) \sim -\frac{R}{r}\frac{k_{\rm p}c_{ss}}{k_{\rm D}b_0}\left[\frac{1}{s}-\frac{r}{R}\sqrt{\frac{\tau}{s}}-\frac{k_{\rm p}c_{ss}}{\kappa_1 b_0}\frac{\Delta\widehat{F}(s)}{s}\right] \tag{3.9}$$

where $\Delta\hat{F}(s) \equiv \hat{F}(s) - \hat{F}(0)$ and the higher order terms in s and $\Delta\hat{F}(s)$ are neglected. For all the approximate theories summarized in section II.C, the leading term of $\Delta\hat{F}(s)$ ($\equiv\Delta\hat{F}_0$) is proportional to $s^{1/2}$, whose explicit form is given in Table 1 of ref 31.Therefore, one concludes that $b(r,t)$ approaches its SS profile, $b_{\rm ss}(r)$, by following a $t^{-1/2}$ power law.

Before proceeding, let us summarize the general behavior of $\Delta b_{\rm rev}(r,t)$ and $\Delta b_{\rm irr}(r,t)$. The reversible component, $\Delta b_{\rm rev}(r,t)$, decreases at short times (due initially to the reaction A + B → C) and passes through a minimum. Then, diffusion restores its initial value at long times, following the ubiquitous $t^{-3/2}$ power law of reversible reactions.[24] In contrast, $\Delta b_{\rm irr}(r,t)$ decreases monotonically to its SS limit because $\partial\Delta b_{\rm irr}(r,t)/\partial t = k_{\rm p}\Delta b_{\rm rev}(r,t) \le 0$. This monotonic behavior of $b(r,t)$ resembles that for the irreversible reaction.[32] $\Delta b_{\rm irr}(r,t)$ and $\Delta b_{\rm rev}(r,t)$ cross at time $t_{\rm c}$. A rough estimate of $t_{\rm c}$ is $1/k_{\rm p}$, which comes from the fact that $\Delta\hat{b}_{\rm rev}(r,s) = \Delta\hat{b}_{\rm irr}(r,s)$ at $s = k_{\rm p}$, which has units of t^{-1}. One can also argue that $t_{\rm c} > t_{\rm m}$, where $t_{\rm m}$ is the time when $\Delta b_{\rm rev}(r,t)$ goes through its minimum.

Varying $k_{\rm p}$ can induce a transition in $b(r,t)$, from monotonic decay to one with a maximum at some $t > t_{\rm m}$. Indeed, its derivative can be written as

$$\frac{\partial}{\partial t}b(r,t) = \frac{\partial}{\partial t}\Delta b_{\rm rev}(r,t) + k_{\rm p}\Delta b_{\rm rev}(r,t) \tag{3.10}$$

When $t > t_{\rm m}$, the first term of the right-hand side is positive whereas $\Delta b_{\rm rev}(r,t) < 0$, so one expects to find a range of $k_{\rm p}$ values for which the derivative of $b(r,t)$ vanishes for $t > t_{\rm m}$ [a maximum in $b(r,t)$], and a critical value, $k_{\rm p}^{\rm cr}$, when the maximum coincides with the minimum.

Finally, the spatial evolution of the concentration gradient can also be characterized by the dynamics of its (reduced) f-width ($0 < f < 1$), which is defined as the dimensionless distance where the depth of the concentration profile is a fraction f of its value at contact:

$$w_f(t) \equiv r_f/R \tag{3.11a}$$

$$\Delta b(r_f,t) = f\Delta b(R,t) \tag{3.11b}$$

The width increases from 1 (at $t = 0$) to $w_f^{\rm ss} = 1/f$ (at SS). These two limits are universal, and independent of the parameters. The behavior in between these limits is dominated by diffusion and thus depends only on $\tau \equiv R^2/D$, and not on the rate coefficients. It can be obtained from eqs 3.8, 3.9, and 3.11 as

$$w_f(t) \sim 1 + {\rm const}\sqrt{t/\tau}, \qquad t \to 0 \tag{3.12a}$$

$$w_f(t) \sim \frac{1}{f+(1-f)/\sqrt{\pi t/\tau}}, \qquad t \to \infty \tag{3.12b}$$

The short-time increase in width reflects the dynamics of $r_f(t)$ which increases from its initial value, $r_f(0) = R$, in the typical diffusive manner for which $(r_f - R)^2 \propto t$. Additional details on this derivation are given in the Appendix A.

IV. Simulation Detail

The BD simulation algorithm for bimolecular reactions developed over the years[24−26,28,31,35] is based on moving particles using random numbers selected from the exact Green function for a single diffusing particle (if remote from the reversible trap) or for a trap−particle pair (when they are close by). We consider N randomly distributed point particles B (diffusion constant $D_{\rm B}$) and a static A/C site of radius R at the origin, all within a big sphere of initial radius $R_{\rm s}(0)$. This radius is larger than the distance a particle covers by diffusion during the entire simulation time, $t_{\rm max}$. At $t > 0$, we consider an analogous sphere of radius $R_{\rm s}(t)$, which a particle cannot traverse during the remaining simulation time, $t_{\rm max} - t$. Therefore, $R_{\rm s}(t)$ is decreased with t, saving on computation time: B particles outside it are no longer moved.

A reactive collision occurs only between A and B, which may lead to association (A + B → C) with a certain probability. B is reflected when it reaches the surface of a bound trap, C. It in turn may dissociate into either A + B or A + P. During a given time step, Δt, these events are treated by selecting random numbers from the exact Green functions describing the evolution of a pair,[31,36] which were pretabulated in look-up tables to speed up the computation. To further reduce computation time, these Green functions are applied only within a reaction zone of radius $r_{\rm s} \ll R_{\rm s}(0)$ around the static enzyme, while B particles outside this zone are moved by three Gaussian random numbers, corresponding to free diffusion but with time-steps which increase with increasing distance from the origin. Thus each particle with $r > r_{\rm s}$ maintains its own "internal time", $t_{\rm in} > t$, which is adjusted to the "real time" t once it crosses the surface of the $r_{\rm s}$ sphere: it is frozen while $t < t_{\rm in}$ then propagated again with the adjusted internal time, $t_{\rm in} = t$.

Additional enhancement in efficiency is obtained by particle elimination methods,[26] where one skips propagation of particles with negligible chance to participate in the reaction. In particular, because every B which reacts with A must first cross the reaction-zone sphere of radius $r_{\rm s}$, the whole initial distribution within $R_{\rm s}(0)$ is mapped onto the surface of the smaller sphere using the solution for diffusion with an absorbing boundary.[26]

Although our algorithm is efficient and accurate for simulating $c(t)$, it can simulate $b(r,t)$ accurately only up to $r = r_{\rm s}$, because for $r > r_{\rm s}$ particles have different $t_{\rm in} > t$ and, additionally, $R_{\rm s}(t)$ shrinks to $r_{\rm s}$ toward the end of the simulation, as $t \to t_{\rm max}$. Therefore, in order to simulate $b(r,t)$ outside the $r_{\rm s}$ sphere, we modify the previous algorithm as follows.

We consider three concentric spheres of radii $r_{\rm s}$, $R_{\rm cut}$, and $R_{\rm s}(t)$, so that $R < r_{\rm s} < R_{\rm cut} < R_{\rm s}(t)$. Within the $r_{\rm s}$ sphere, particles are propagated with the minimal time step using the "Brownian propagator" obtained from the exact Green functions. Between $r_{\rm s}$ and $R_{\rm cut}$, these are propagated by the simpler, "Gaussian propagator" (still utilizing the minimal time step). Outside the $R_{\rm cut}$ sphere we use the Gaussian propagator with distance-dependent time steps. Once entering this sphere from the outside, the particle is frozen until the real time catches up with its $t_{\rm in}$. Thus, all the particles within the $R_{\rm cut}$ sphere have a synchronized internal time $t_{\rm in} = t$. These modifications are realized as follows.

First, we modify $R_{\rm s}(t)$ so that $R_{\rm s}(t) \ge R_{\rm cut}$ and it shrinks to $R_{\rm cut}$ (instead of to $r_{\rm s}$) as $t \to t_{\rm max}$. This is achieved by defining

$$R_{\rm s}(t) = R_{\rm cut} + \beta\sqrt{2D_B(t_{\rm max}-t)} \tag{4.1}$$

where $\beta \approx 8$ [thus ensuring that a particle cannot move across the $R_{\rm s}(t)$ sphere during $t_{\rm max} - t$].[24−26,28,31,35] Similarly, the initial

uniform distribution of B's in infinite space is mapped onto the surface of the R_{cut} sphere (instead of that of the r_s sphere).

The time step for particle motion is modified as follows. For $r \le R_{cut}$ it assumes a minimal and fixed value, $\tau_0 = (r_s - R)^2/(2\beta^2 D_B)$. Outside this sphere, each particle has its own "internal time step", Δt_{in}, which is modified to increase with the distance from the R_{cut} sphere according to $\Delta t_{in} = k\tau_0$, where k is the integer part of

$$\max\left[1, \frac{(r-R_{cut})^2}{2\beta^2 D_B \tau_0}\right] = \max\left[1, \left(\frac{r-R_{cut}}{r_s-R}\right)^2\right] \qquad (4.2)$$

This ensures that a particle arriving at R_{cut} would not penetrate deep inside the R_{cut} sphere during a single time step, Δt_{in}.

A reasonable choice of R_{cut} is essential for long-time simulations because computational efficiency decreases as R_{cut} increases. Because a particle may diffuse a distance $\sqrt{(6D_B t_{max})}$ during t_{max}, it is reasonable to set $R_{cut} = r_s + \sqrt{(6D_B t_{max})}$. The additional cost paid by adopting this R_{cut} is acceptable when t_{max} is not large. However, it increases rapidly with t_{max} (roughly as $t_{max}^{3/2}$) so that eventually the simulation becomes prohibitively expensive. Therefore, we set the upper limit of R_{cut} as $w_{1/4}^{ss}R = 4R$. Thus, our choice of R_{cut} is

$$R_{cut} = \min\{r_s + \sqrt{6D_B t_{max}}, 4R\} \qquad (4.3)$$

With the above modifications, we were able to simulate $b(r,t)$ efficiently and accurately for $r \le R_{cut}$. The concentration profiles were calculated with spatial resolution of $\Delta r/R = 2 \times 10^{-4}$ for short times, and 1×10^{-3}, 2×10^{-3}, or 1×10^{-2} for longer times. These were then averaged over a sufficiently large number of simulations to produce smooth results.

V. Results

A. Parameters. Here we explain the choice of the parameters for which the BD simulations were performed. Consider dimensionless units, in which distance is in units of the contact radius, R, and time in units of the diffusion time, $\tau \equiv R^2/D_B$. For convenience, define also a characteristic concentration $c_R \equiv (4\pi R^3)^{-1}$, so that concentrations are given in units of c_R. The diffusion-control rate constant, in these units, is $k_D \equiv 4\pi D_B R = (c_R\tau)^{-1}$. We also write the three rate parameters as dimensionless quantities: Unimolecular rate parameters in units of τ^{-1} and the bimolecular rate parameter in units of k_D. To reduce the number of adjusted parameters, we have fixed the unimolecular rate parameters: $\kappa_2\tau = 1$ and $k_p\tau = 10$. This leaves κ_1 and b_0 to be varied.

We consequently investigate MM kinetics using two sets of parameters: (A) $\kappa_1/k_D = 5$ and $b_0/c_R = 1$; (B) $\kappa_1/k_D = 50$ and $b_0/c_R = 10$.

Thus in case (B) the enzyme is more heavily loaded with substrate. As seen from eq 2.8a, c_{ss} increases as $\kappa_1 b_0$ becomes larger, and so does the competition between ligands for enzyme binding. This leads to a more stringent test for the approximate many-body theories.

Now selecting time and distance units is equivalent to selecting physical values for R and D_B. This then sets the physical values of all the above-mentioned parameters. We present this as calibration curves in Figure 1. The gray regions correspond to the physically relevant range for the parameters, hence R and τ should be chosen so that all calibration curves are inside these regions. With this restriction, a single dimensionless simulation can depict many physically relevant systems.

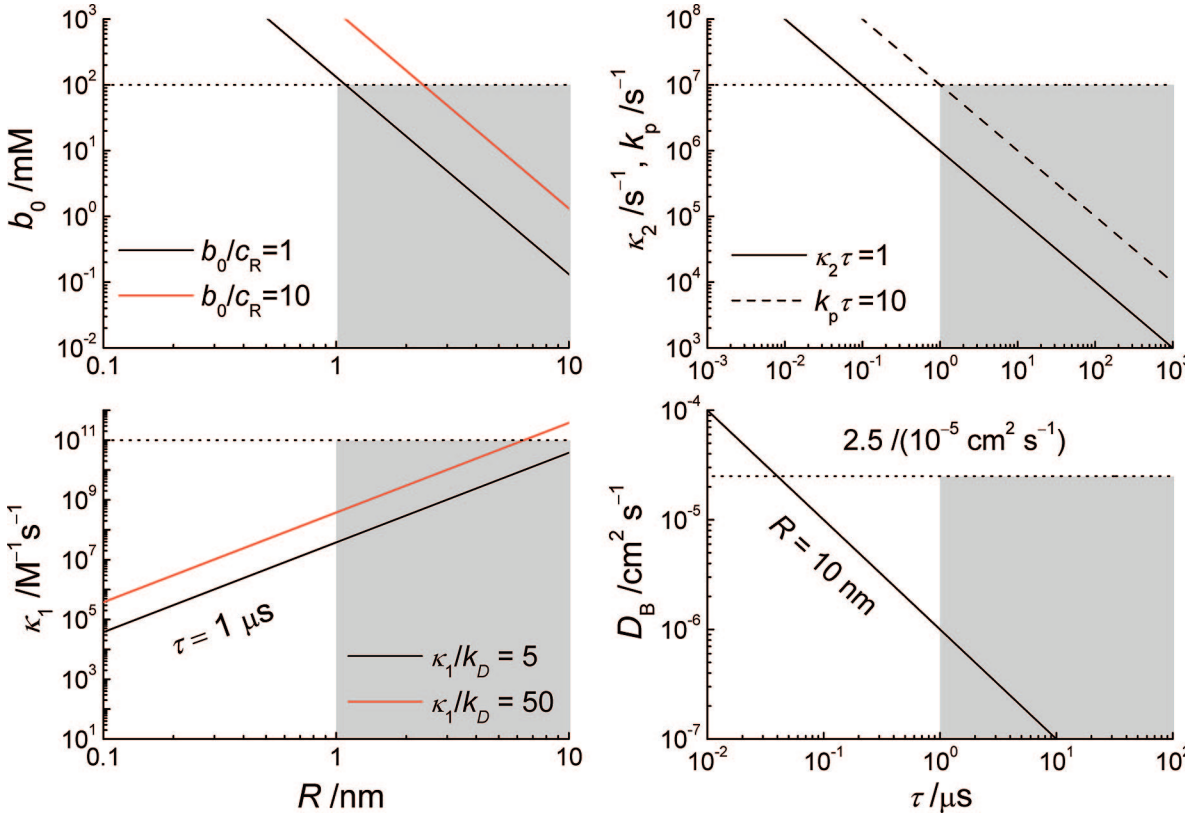

Figure 1. Calibration curves showing the physical values of the parameters as a function of the choice of R and τ. Gray rectangles correspond roughly to the experimentally accessible regime. For the R dependence (left panels) we show cases (A) and (B) as black and red lines, respectively.

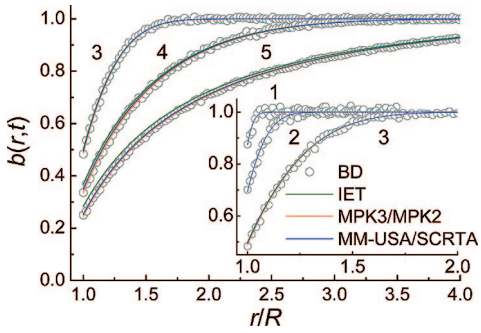

Figure 2. Concentration profiles, $b(r,t)$, for an initially constant substrate concentration and an unbound enzyme are depicted as a function of distance for several times ($t/\tau = 6.53 \times 10^{i-5}$, for the indicated values of $i = 1-8$). The MM mechanism was simulated (circles) for the following dimensionless parameter values: $\kappa_2\tau = 1$, $k_p\tau = 10$, $\kappa_1/k_D = 5$, and $b_0/c_R = 1$. The physical values of the parameters can be obtained from our calibration curves given in Figure 1 once values for R and τ are selected. The inset shows the short-time behavior. Lines depict various theoretical approximations, calculated by inverse LT of eq 3.3 using the DFF of section II.C. Because all the theoretical lines are so close in the present case, MPK3/MET and SCRTA are omitted for clarity (they coincide with MPK2/KT and MM-USA, respectively).

Typical values of parameters for enzymatic reactions in solution are summarized in ref 31. An enzyme radius is in the range of 1−10 nm, substrate diffusion constant is below that of liquid water, typical concentrations are under 100 mM, bimolecular rate parameters under 10^{11} M^{-1} s^{-1}, and unimolecular rate parameters under 10^7 s^{-1}. For our choice of κ_2 and k_p, this means that $\tau > 1$ μs. For example, if $R = 5$ nm then $b_0 = 1.06$ and 10.6 mM for cases (A) and (B), respectively. If also $\tau = 1$ μs, then $\kappa_1 = 4.73 \times 10^9$ and 4.73×10^{10} M^{-1} s^{-1} for these two cases. For these choices of R and τ, $D_B \approx 2.5 \times 10^{-7}$ cm^2 s^{-1}, which is a reasonable value for diffusion inside the living cell, where viscosity and, even more so, microscopic obstacles slow down translational motion.[11,12]

B. Concentration Profiles. We have simulated the concentration profiles for the MM reaction starting from an unbound enzyme and a uniform substrate concentration, and compared the results with the theoretical predictions of the IET, MKP3/MET, MPK2/KT, SCRTA, and MM-USA approximations. For the different parameter sets, $b(r,t)$ shows qualitatively different behavior. In case (A) it shows irreversible reaction-like behavior, in which concentrations near a trap decrease monotonically to SS, and all theories agree well with the simulations. In the second case $b(r,t)$ shows a nonmonotonic behavior with time, and the theories deviate from one another and from the simulations.

The concentration profiles for case (A) are shown in Figure 2 for short (inset) and intermediate times, whereas results for longer times are shown in Figure 3. Starting with $b(r,0) = 1$, a concentration gradient develops with time and approaches monotonically its SS limit. In this limit, $b(r,t)$ assumes a simple hyperbolic dependence on r, $\Delta b(r,t) \propto R/r$, but its proportionality constant has a complicated dependence on the kinetic parameters, as obtained in eq 3.4.

Superimposed on the simulation data (circles), we plot the theoretical dependencies (lines) calculated by inverse LT of $\hat{b}(r,s)$ with the appropriate DFF, eq 2.10. The theoretical concentration profiles are identical at $t = 0$, when $b(r,0) = 1$, and tend to diverge from each other at longer times. However, in the present case the difference between the various theories is so small that they essentially coincide. Only IET, an approximation valid for small b_0, shows some divergence in the SS limit.

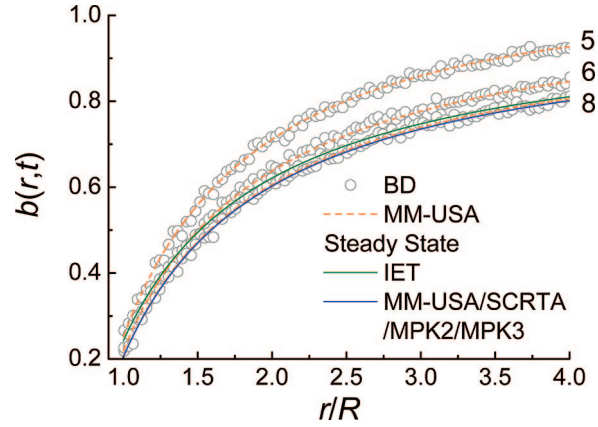

Figure 3. Same as Figure 2 at longer times (dashed lines) and at SS (full lines). The curve with $i = 8$ is almost in the SS limit. Except for the IET, all theories predict indistinguishable $b_{ss}(r)$ for this parameter set.

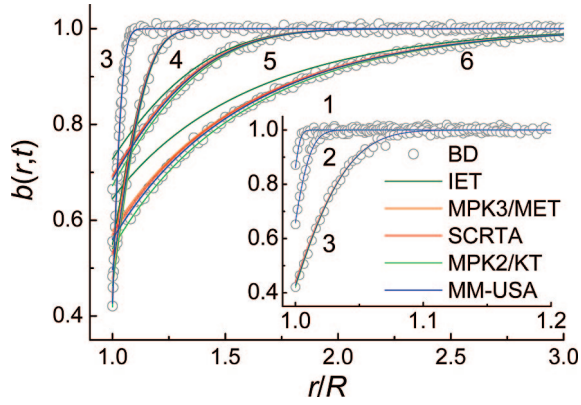

Figure 4. Same as Figure 2 except that $\kappa_1/k_D = 50$, and $b_0/c_R = 10$. The numbers, i, beside the curves indicate that $t/\tau = 7.66 \times 10^{i-7}$.

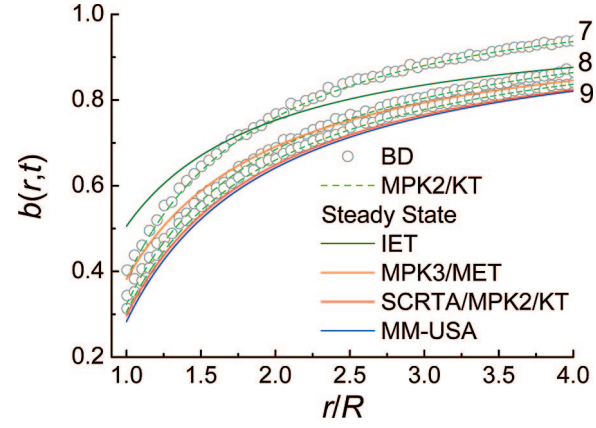

Figure 5. Same as Figure 4 at longer times (dashed lines) and at SS (full lines). Theories deviate from one another significantly for this parameter set.

For case (B) the simulated concentration profiles (circles) are shown in Figure 4 up to intermediate times, and for times closer to SS in Figure 5. The theoretical lines increasingly deviate from one another as SS is approached. The least accurate is the IET. It is a small b_0 approximation applied here at large b_0. MPK3/MET is somewhat better, but it still approaches the wrong SS limit. The other three theories, MPK2/KT, SCRTA, and MM-USA, are closer to the simulation data. At SS, MPK2/KT and SCRTA are identical because they have identical $\hat{F}(0)$. However,

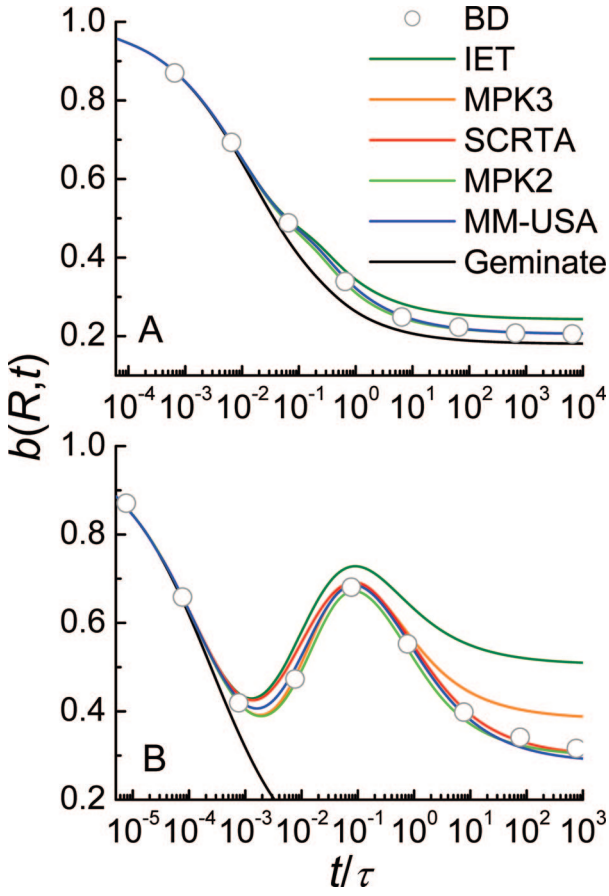

Figure 6. Time dependence of $b(R,t)$ for the MM mechanism. For the first parameter set (panel A), it decreases monotonically. For the second parameter set (panel B), it shows a nonmonotonic evolution at intermediate times.

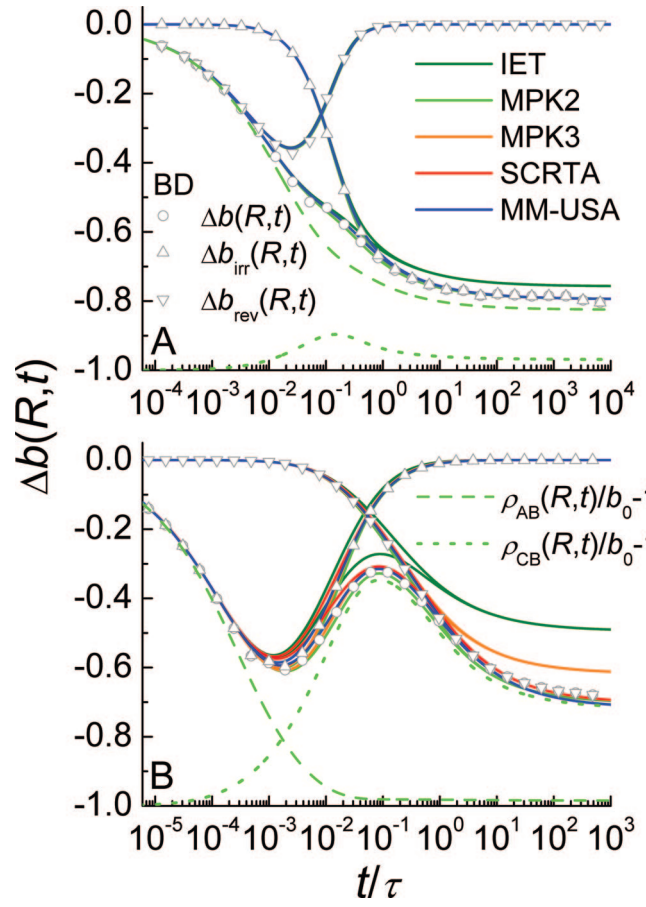

Figure 7. Decomposition of $\Delta b(R,t)$ into its reversible and irreversible components, $\Delta b_{rev}(R,t)$ and $\Delta b_{irr}(R,t)$, respectively. For the first parameter set (panel A), the contribution from $\Delta b_{rev}(R,t)$ is small so that $b(R,t)$ decreases monotonically. For the second parameter set (panel B), its contribution is large, thus $b(R,t)$ shows nonmonotonic evolution. An alternate decomposition of $\Delta b(R,t)$ into $\rho_{AB}(R,t)/b_0 - 1$ and $\rho_{CB}(R,t)/b_0 - 1$, obtained by the inverse LT of eqs B6 for MPK2/KT is shown by the dashed and dotted lines, respectively.

at intermediate times MPK2/KT is better, as already noted for $c(t)$ in our previous work.[31]

An interesting effect that is observed here is the nonmonotonic time dependence of $b(r,t)$ near the enzyme. This can be seen in lines 3, 4, and 5 in Figure 4 for $r/R < 1.1$. Ligand concentration close to the enzyme first decreases and then increases, whereas far from the enzyme it decreases monotonically to SS as before.

The maximal effect is manifested for $r = R$. Therefore, we compare $b(R,t)$ for the two parameter sets in the two panels of Figure 6. In case (A), $b(R,t)$ decays monotonically to its SS limit, $b_{ss}(R) = 0.205$, and all the theories (except IET) agree with the simulation. In (B) there is a strong nonmonotonic behavior at intermediate times, even though $b_{ss}(R) = 0.29$ is only moderately larger than before. A maximum in $b(R,t)$ now appears when $t/\tau \approx 8.5 \times 10^{-2}$. As shown above, the theories deviate more for this parameter set, with IET and MPK3/MET converging to the wrong SS solution.

For comparison, we also show the geminate pair solution ($b_0 \rightarrow 0$ limit), which was obtained analytically in ref 36 (set $k_0 = k_p$ and $k'_0 = 0$ there). It is equivalent to the case of many B particles which are independent of each other, and then the single-particle probability density becomes identical with the many-particle concentration profile.[34] Thus, there are no (many-body) competition effects in this case. This provides the correct short-time behavior, valid as long as the enzyme interacts with only one (the first) ligand. As time proceeds, many-body competition leads to deviations from pair dynamics. These are much larger in case (B) due to the enhanced competition effects for higher concentrations.

C. Contact Concentration. To understand the origin of the nonmonotonic time dependence, we plot in Figure 7 the two components of $\Delta b(R,t)$ in eq 3.6, namely $\Delta b_{rev}(R,t)$ and $\Delta b_{irr}(R,t)$. These were calculated by inserting $\hat{c}(s)$ into eqs 3.7 and inverting the LT. Alternately, the simulated $c(t)$ (data not shown) and $G(R,t|R)$ are convoluted to calculate these components. In agreement with previous simulations of the reversible ABC reaction (Figure 8 in ref 24), $\Delta b_{rev}(R,t)$ first decreases, passes through a minimum and then returns to its initial value. The decrease is due to substrate binding, whereas the increase is due to their replenishment by diffusion. Thus, a sizable minimum arises when diffusion is slow as compared to reversible binding. When only the first reversible step is operative, at most one substrate is bound and this cannot cause a permanent depletion of the concentration profile.

The second component, $\Delta b_{irr}(R,t)$, does create a permanent substrate depletion near the enzyme because it continuously processes B's into P's. The rate of this enzyme turnover is dictated by k_p. When it is sufficiently small, there is time for $b(R,t)$ to recover before the turnover of the second substrate and a maximum is thus observed. When k_p is large, there is no time for diffusion to compensate for the binding of the first ligand before the second one is processed, and no maximum is observed. Thus, we expect a transition from nonmonotonic to monotonic behavior as k_p is increased. The above qualitative

interpretation agrees with the general behavior of $b(r,t)$ which was given in section III.

Alternatively, $b(R,t)$ can be decomposed into $\rho_{AB}(R,t)$ and $\rho_{CB}(R,t)$, which are shown as the dashed and dotted lines in Figure 7. It is seen that $\rho_{AB}(R,t)$ provides another short-time approximation to $b(R,t)$, which is comparable to $\Delta b_{rev}(R,t)$ when $b(R,t)$ is monotonic. In this case, the contribution of $\rho_{CB}(R,t)$ is small, whereas the peak in the nonmonotonic case arises from that of $\rho_{CB}(R,t)$. This confirms our interpretation that the peak appears due to replenishment of substrate molecules around the bound enzyme before substrate turnover. A discussion of these pair distribution functions is given in Appendix B.

A condition for observing nonmonotonic behavior comes from time-scale separation for three processes. The fastest component is reversible binding, whose characteristic time t_b is given by

$$\frac{t_b}{\tau} \approx \frac{1}{\lambda_0 \tau} = \left(\frac{b_0}{c_R} \frac{\kappa_1}{k_D} + \kappa_2 \tau \right)^{-1} \tag{5.1a}$$

To observe a sizable dip in the concentration profile, binding should be faster than diffusion, $t_b < \tau$ (or $\lambda_0 \tau > 1$). Indeed, for cases (A) and (B) we have $t_b/\tau = 0.167$ and 2.00×10^{-3}, respectively.

Next, we estimate more accurately the characteristic recovery time, t_r, of $\Delta b_{rev}(R,t)$ due to diffusion. From its long-time behavior we find in Appendix C that

$$t_r/\tau = 1/(\lambda_0 \tau)^{2/3} \tag{5.1b}$$

For parameter sets (A) and (B), $t_r/\tau = 0.302$ and 1.59×10^{-2}, respectively. Hence $t_b < t_r < \tau$ in both cases, so that the bimolecular step is indeed in the diffusion-control limit. The characteristic time for the second, irreversible step in the MM mechanism is

$$t_p/\tau \equiv 1/(k_p \tau) \tag{5.1c}$$

Since $t_p/\tau = 0.1$ here, we find $t_p < t_r$ for case (A) vs $t_p \gg t_r$ for case (B), when nonmonotonic behavior is observed. This is due to slow enzyme turnover as compared with recovery. Therefore, the condition for observing nonmonotonic behavior is

$$k_p \tau \le (\lambda_0 \tau)^{2/3} \tag{5.2}$$

The k_p-dependent behavior of $b(R,t)$ for $\lambda_0 \tau = 6$ and 501 [the same as those for parameter sets (A) and (B), respectively] are shown in Figure 8. For small k_p, $b(R,t)$ shows nonmonotonic behavior and its minimum due to reversible binding appears around $t/\tau \approx 1/[(\lambda_0 + k_p)\tau]$. As k_p increases, a kinetic transition occurs at its critical value k_p^{cr}. For parameter sets (A1) and (A2), $k_p^{cr}\tau \approx 3.345$ and 3.543. For parameter sets (B1) and (B2), $k_p^{cr}\tau \approx 1.574 \times 10^2$ and 1.537×10^2. At the transition we observe a plateau, when the temporal change in $b(R,t)$ is negligible, extending from $t/\tau \approx 1/(3k_p^{cr}\tau)$ to $t/\tau \approx 5/(6k_p^{cr}\tau)$. This agrees with our prediction that $\partial b(r,t)/\partial t \approx 0$ around $t/\tau = 1/(k_p^{cr}\tau)$ given in section III. For $k_p > k_p^{cr}$ the maximum of $b(R,t)$ disappears and its behavior becomes monotonic.

We find that $k_p^{cr}\tau = (\lambda_0 \tau)^{2/3}$ gives a good estimate of the critical value of $k_p\tau$ up to $\lambda_0 \tau \approx 10$. For parameter sets (A1) and (A2), $k_p^{cr}\tau/(\lambda_0\tau)^{2/3} \approx 1.013$ and 1.073, respectively. However, this criterion deteriorates for larger $\lambda_0\tau$. Thus, for cases (B1) and (B2) we find that $k_p^{cr}\tau/(\lambda_0\tau)^{2/3} \approx 2.495$ and 2.437, respectively.

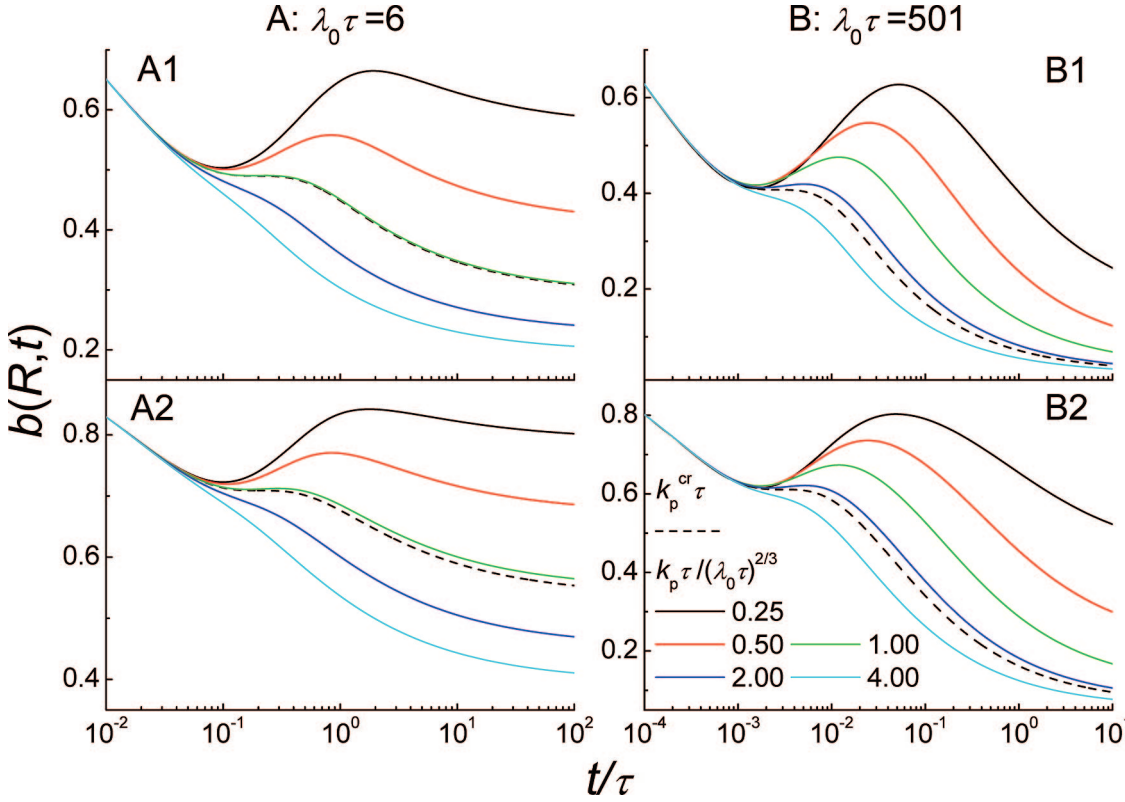

Figure 8. Dependence of the normalized substrate concentration profile near the enzyme, $b(R,t)$, on the (enzymatic) turnover rate parameter, k_p. Calculated from the MM-USA theory, which was shown above to be essentially exact as compared to simulation. Two subsets for a given $\lambda_0\tau$ are shown together for comparison: $\lambda_0\tau = 6$ and 501 for (A) and (B), respectively. For sets (A1) and (B1), κ_1/k_D, b_0/c_R, and $\kappa_2\tau$ are the same as those used in the simulations. These are more symmetric for sets (A2) $\kappa_1/k_D = 2$, $b_0/c_R = 2$, and $\kappa_2\tau = 2$, and (B2) $\kappa_1/k_D = 21.9$, $b_0/c_R = 21.9$, and $\kappa_2\tau = 21.39$. As k_p increases, the maximum in $b(R,t)$ disappears and its time dependence becomes monotonic. The dashed curves depict $b(R,t)$ at the transition, exhibiting the emergence of a plateau at the critical turnover number, $k_p = k_p^{cr}$.

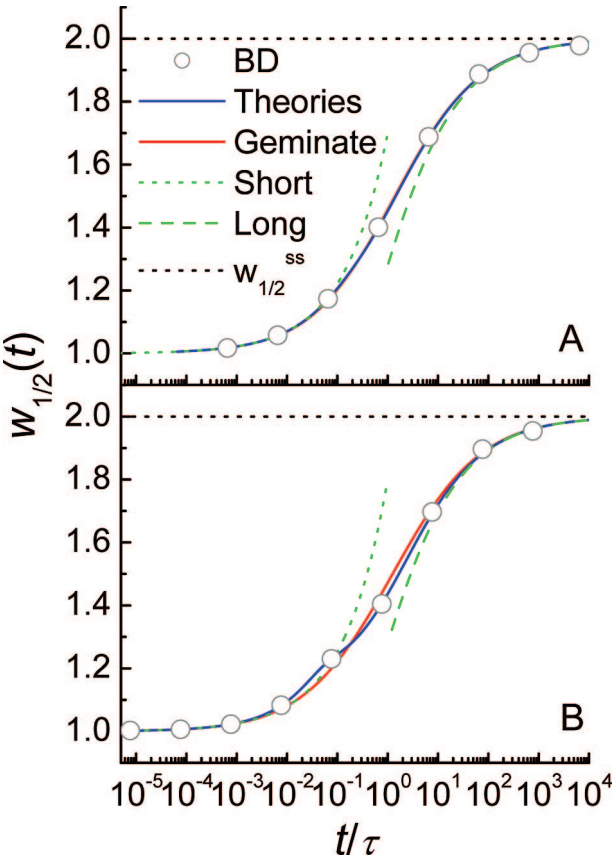

Figure 9. Time dependence of the half-width of the concentration profile, $w_{1/2}(t)$. The short- and long-time behaviors are calculated from eqs 3.12a and 3.12b, respectively. Here all the approximate theories overlap, even the geminate solution, which deviates only for the second parameter set (panel B).

D. Width Dynamics. A measure of the shape of the concentration profiles is their spatial width. In Figure 9, we show the dynamics of the half-width, $w_{1/2}(t)$, depicting broadening of the concentration profile with time. Simulation data are obtained by solving eqs 3.11 numerically from a high order polynomial fit to $b(r,t)$. As pointed out in section III, $w_{1/2}(t)$ depends weakly on all the parameters except τ. Consequently, all the theories coincide here with the simulation data. In addition, the competition effect is only discernible through a small kink at intermediate times in panel B. For comparison, $w_{1/2}(t)$ for the geminate solution is also shown. It exhibits only small deviations from the simulation data, when many-body effects become important (Figure 9B). Its short- and long-time behaviors, eqs 3.12, are shown as dashed lines. Free diffusion in solution seems to account for most of the widening process, which is therefore much less instructive than $b(R,t)$ with respect to the underlying kinetic mechanism.

VI. Concluding Remarks

There have been very little experimental or theoretical studies of substrate concentration profiles which develop near an activated enzyme. Evidently, when the enzyme is idle, the concentration profile around it is uniform. After it is activated, substrates are depleted near the enzyme. We have studied this effect both computationally and theoretically. Computationally, we have employed our accurate BD algorithm for studying the MM mechanism.[31] Theoretically, we have utilized modern many-particle theories which show remarkable agreement with simulations.[14,18,21]

Of prime interest is the SS concentration profile of substrates near an enzyme. We find the expected hyperbolic distance dependence,[32] R/r, but its prefactor is a complicated function of the various rate parameters. As eq 3.4 shows, many-particle effects enter into the SS solution through the $s \to 0$ limit of the DFF, $\hat{F}(0)$. This factor then enters into the generalized Michaelis constant, K_M, modifying the SS fraction of bound enzyme, c_{ss}, and hence the effective irreversible rate-constant, $k_p c_{ss}$ in the SS diffusion equation 3.5. Only when diffusion is fast, one obtains the reaction control limit in which $\hat{F}(0) = 1$, and K_M assumes its familiar form from basic enzymological kinetics.[1] Yet, within the living cell, molecules may be crowded, so that diffusion becomes rate limiting.[11,12] Then $\hat{F}(0) \neq 1$ and effects discussed herein cannot be neglected.

Before a SS concentration profile is established, there is a transient phase during which the initially uniform substrate concentration evolves into the final SS profile. We have derived (approximate) analytic expressions for the LT of the concentration profiles, $\hat{b}(r,s)$, eq 3.3, which were inverted numerically to yield $b(r,t)$. In parallel, we have extended our previously reported BD simulation routine for MM kinetics[31] so as to calculate, besides the enzyme binding probability, $c(t)$, also the full concentration profile. Comparison between the two approaches indicated that of the various theories, those with "uniform" convergence properties (particularly MPK2/KT and MM-USA) are in excellent agreement with simulation.

Our study revealed an interesting property of the concentration profiles, which undergo a "kinetic transition" as a function of the enzyme turnover rate parameter, k_p. The effect is manifested near the surface of the enzyme, where competition effects are most pronounced. When k_p is large, substrate molecules which arrive at the enzyme surface are processed immediately, so that $b(R,t)$ decays monotonically to its SS value. However, when k_p is small there is time for "quasi-equilibrium" in the first, reversible step of the MM mechanism. Diffusion now replenishes the substrate near the enzyme before the product is released. This leads to a minimum in $b(R,t)$. Subsequently, product release allows processing of more substrate molecules, so that $b(R,t)$ decreases again, thus attaining its SS limit in a nonmonotonic fashion. We have estimated the condition for the nonmonotonic behavior as $k_p\tau \leq (\lambda_0\tau)^{2/3}$, which is valid up to $\lambda_0\tau \approx 10$.

In low dimensions, there have been several experimental studies on the broadening of concentration profiles based on fluorescence spectroscopy.[37] We are not aware of quantitative studies of substrate concentration profiles near an activated enzyme, particularly under intercellular conditions which may slow down diffusion and lead to acute competition for substrate molecules. Yet, this is a physically meaningful quantity, which is presently best accessed through theory and simulation. Reliable modern methods for multiparticle diffusive kinetics have yielded predictions which must now await experimental verification.

Acknowledgment. S.P. thanks the Golda Meir Fellowship Fund for financial support. This research was supported in part by The Israel Science Foundation (grant no. 191/03). The Fritz Haber Center is supported by the Minerva Gesellschaft für die Forschung, München, FRG.

Appendix A: Short-Time Behavior of Width Dynamics

Here, we derive the short-time behavior of $w_f(t)$ using the Smoluchowski−Collins−Kimball (SCK) model for irreversible reactions,[32] which reproduces well the short-time dynamics of

$b(r,t)$ for the MM mechanism. Because $G(r,t|R)$ is a dominating factor of the broadening dynamics, one can obtain an essentially identical short-time behavior from more sophisticated theories. Therefore, it suffices to provide that of the SCK model.

For the SCK model with a radiation boundary condition, $\alpha(t) = -\kappa_1[B](R,t)$ and $\Delta b(r,t)$ is given by[32]

$$\Delta b(r,t) = -\frac{\kappa_1}{(\kappa_1+k_D)}\frac{R}{r}\left[\mathrm{erfc}\left(\frac{r/R-1}{2\sqrt{z}}\right) - W\left(\frac{r/R-1}{2\sqrt{z}}, \frac{\kappa_1+k_D}{k_D}\sqrt{z}\right)\right] \quad \text{(A1)}$$

where $z = t/\tau$ and $W(x,y) = \exp(2xy + y^2)\,\mathrm{erfc}(x + y)$. From eqs 3.11, one can obtain

$$fw_f = \frac{\mathrm{erfc}\left(\frac{w_f-1}{2\sqrt{z}}\right) - W\left(\frac{w_f-1}{2\sqrt{z}}, \frac{\kappa_1+k_D}{k_D}\sqrt{z}\right)}{1 - W\left(0, \frac{\kappa_1+k_D}{k_D}\sqrt{z}\right)} \quad \text{(A2)}$$

At short times, the numerator and the denominator in the above equation behave as

$$\mathrm{erfc}(u) - W(u, v\sqrt{z}) \sim v\sqrt{\frac{z}{\pi}}\frac{e^{-u^2}}{u^2}\left[1 - \frac{2v}{u}\sqrt{z} - \frac{3}{u^2} + O(z^2)\right] \quad \text{(A3)}$$

$$1 - W(0, v\sqrt{z}) \sim 2v\sqrt{\frac{z}{\pi}}\left[1 - v\frac{\sqrt{\pi z}}{2} + v^2\frac{4z}{3} + O(z^{3/2})\right] \quad \text{(A4)}$$

where $u = (w_f - 1)/(2\sqrt{z})$ and $v = 1 + \kappa_1/k_D$. Substituting these into eq A2, one can obtain

$$fw_f \approx \frac{\exp(-u^2)}{2u^2}\left[1 + v\frac{\sqrt{\pi z}}{2} + O(z)\right] \quad \text{(A5)}$$

Taking the $t \to 0$ limit in the left-hand side, $w_f \approx 1$, and we obtain

$$2fu^2 \approx \exp(-u^2) \quad \text{(A6)}$$

This equation can be solved numerically for u. With this constant value inserted, eq A5 yields $w_f(t) - 1 \propto \sqrt{z}$.

Appendix B: Pair Distribution Function

Here, we present the pair distribution functions, $\hat{\rho}_{AB}(r,s)$ and $\hat{\rho}_{CB}(r,s)$, for the IET, SCRTA, MKP2/KT, and MPK3/MET. In these approximate theories, the infinite hierarchy of eqs 2.2 is truncated at the three-particle level. The approximated quantity is an extension of $\alpha(t)$ to the next level of hierarchy

$$\alpha_B(r,t) \equiv -\kappa_1\rho_{ABB}(r,R,t) + \kappa_2\rho_{CB}(r,t) \quad \text{(B1)}$$

In the SCRTA, MPK2/KT, and MPK3/MET, it is approximated as[15,16,18]

$$\hat{\alpha}_B(r,s) = b_0\hat{\alpha}(s) - k_1b_0\Delta\hat{\rho}_{AB}(r,s) + k_2\Delta\hat{\rho}_{CB}(r,s) \quad \text{(B2)}$$

where the effective rate coefficients, k_i, are calculated as described in section II.C. The deviation functions for the pair distribution functions from their chemical kinetic limits are defined as

$$\Delta\rho_{AB}(r,t) \equiv \rho_{AB}(r,t) - b_0a(t) \quad \text{(B3a)}$$

$$\Delta\rho_{CB}(r,t) \equiv \rho_{CB}(r,t) - b_0c(t) \quad \text{(B3b)}$$

They initially satisfy

$$\Delta\rho_{AB}(r,0) = \Delta\rho_{CB}(r,0) = 0 \quad \text{(B4)}$$

Substituting eqs B2 and B3 into the LT of eqs 2.2b and 2.2c one finds that the deviation functions obey the reaction diffusion equations:

$$(s - \mathcal{L}_r)\Delta\hat{\rho}_{AB}(r,s) = -k_1b_0\Delta\hat{\rho}_{AB}(r,s) + (k_2+k_p)\Delta\hat{\rho}_{CB}(r,s) + \hat{\alpha}(s)\frac{\delta(r-R)}{4\pi R^2} \quad \text{(B5a)}$$

$$(s - \mathcal{L}_r)\Delta\hat{\rho}_{CB}(r,s) = k_1b_0\Delta\hat{\rho}_{AB}(r,s) - (k_2+k_p)\Delta\hat{\rho}_{CB}(r,s) \quad \text{(B5b)}$$

Note that while these equations are approximate, their sum is the formally exact eq 3.2.

The solutions of the above equations have the general form:

$$\frac{\Delta\hat{\rho}_{AB}(r,s)}{\hat{\alpha}(s)} = \mu\hat{G}(r,s|R) + (1-\mu)\hat{G}(r,s_p+\lambda|R) \quad \text{(B6a)}$$

$$\frac{\Delta\hat{\rho}_{CB}(r,s)}{\hat{\alpha}(s)} = (1-\mu)[\hat{G}(r,s|R) - \hat{G}(r,s_p+\lambda|R)] \quad \text{(B6b)}$$

with μ defined in eq 2.14. The above equations are approximate but they sum to the formally exact eq 3.3.

For the IET, which is valid only in the low concentration limit, $\mu = 1$. For the SCRTA, MPK2/KT, and MPK3/MET, the effective rate coefficients are calculated as described in section II.C. For the MM-USA, one can obtain $\Delta\hat{\rho}_{AB}(R,s)$ and $\Delta\hat{\rho}_{CB}(R,s)$ from those for the SCRTA by further replacing the second term of the right-hand side in eqs B6 as described in section II.C.

When $b(R,t)$ shows nonmonotonic behavior, one can estimate numerically the time for the maximum and minimum by solving the equations: $d\rho_{CB}(R,t)/dt = 0$ and $\rho_{AB}(R,t) = \rho_{CB}(R,t)$, respectively. The estimated times become more accurate as k_p/λ_0 decreases (see Figure 7B).

Appendix C: Characteristic Recovery Time of $\Delta b_{rev}(R,t)$

As discussed in section V.C, nonmonotonic evolution of $b(R,t)$ occurs when the time scale, t_r, for recovery of $b(R,t)$ is smaller than that for the enzymatic turnover, $t_p = 1/k_p$. Here, we estimate t_r under an assumption of time scale separation.

From eqs 2.7, 2.11a, and 3.7a, $\Delta\hat{b}_{rev}(R,s)$ at small s can be written as

$$\Delta\hat{b}_{rev}(R,s) \sim -\frac{\kappa_1}{k_D}t_b(1 - \sqrt{\tau s}) \quad \text{(C1)}$$

where the binding time, t_b, is defined as

$$t_b \equiv 1/[\lambda_0 + k_p\hat{F}(0)] \quad \text{(C2)}$$

We now assume that due to the separation of time scales we have

$$\lambda_0 \gg k_p\hat{F}(0) \quad \text{(C3)}$$

so that t_b is approximated as $1/\lambda_0$, see eq 5.1a.

Inverting eq C1 into the time domain, we obtain the long-time behavior of $\Delta b_{rev}(R,t)$ as

$$\Delta b_{\mathrm{rev}}(R,t) \sim -\frac{\kappa_1/k_{\mathrm{D}}}{2\sqrt{\pi}}\frac{t_{\mathrm{b}}}{\tau}\left(\frac{\tau}{t}\right)^{3/2} \tag{C4}$$

This suggests defining a recovery time

$$\frac{t_{\mathrm{r}}}{\tau} \equiv \left(\frac{t_{\mathrm{b}}}{\tau}\right)^{2/3} \tag{C5}$$

as given in eq 5.1b. This result was verified numerically.

References and Notes

(1) Fersht, A. *Structure and Mechanism in Protein Science: A Guide to Enzyme Catalysis and Protein Folding*, 1st ed.; Freeman: New York, 1999.
(2) Engasser, J.-M.; Horvath, C. *J. Theor. Biol.* **1973**, *42*, 137.
(3) Atkins, G. L.; Nimmo, I. A. *Biochem. J.* **1975**, *149*, 775.
(4) Clark, D. S.; Bailey, J. E. *Biotechnol. Bioeng.* **1983**, *25*, 1027.
(5) Agmon, N. *J. Theor. Biol.* **1985**, *113*, 711.
(6) Arrio-Dupont, M.; Béchet, J.-J. *Biochimie* **1989**, *71*, 833.
(7) Nelsestuen, G. L.; Martinez, M. B. *Biochemistry* **1997**, *36*, 9081.
(8) Agmon, N. *J. Phys. Chem. B* **2000**, *104*, 7830.
(9) English, B. P.; Min, W.; van Oijen, A. M.; Lee, K. T.; Luo, G.; Sun, H.; Cherayil, B. J.; Kou, S. C.; Xie, X. S. *Nat. Chem. Biol.* **2006**, *2*, 87.
(10) Min, W.; Gopich, I. V.; English, B. P.; Kou, S. C.; Xie, X. S.; Szabo, A. *J. Phys. Chem. B* **2006**, *110*, 20093.
(11) Luby-Phelps, K. *Int. Rev. Cytol.* **2000**, *192*, 189.
(12) Dayel, M. J.; Hom, E. F. Y.; Verkman, A. S. *Biophys. J.* **1999**, *76*, 2843.
(13) Lee, S.; Karplus, M. *J. Chem. Phys.* **1987**, *86*, 1883.
(14) Sung, J.; Lee, S. *J. Chem. Phys.* **1999**, *111*, 796.
(15) Sung, J.; Lee, S. *J. Chem. Phys.* **1999**, *111*, 10159.
(16) Sung, J.; Lee, S. *J. Chem. Phys.* **2000**, *112*, 2128.
(17) Ivanov, K. L.; Lukzen, N. N.; Kipriyanov, A. A.; Doktorov, A. B. *Phys. Chem. Chem. Phys.* **2004**, *6*, 1706.
(18) Gopich, I. V.; Szabo, A. *J. Chem. Phys.* **2002**, *117*, 507.
(19) Yang, M.; Lee, S.; Shin, K. J. *J. Chem. Phys.* **1998**, *108*, 117.
(20) Yang, M.; Lee, S.; Shin, K. J. *J. Chem. Phys.* **1998**, *108*, 8557.
(21) Yang, M.; Lee, S.; Shin, K. J. *J. Chem. Phys.* **1998**, *108*, 9069.
(22) Gopich, I. V.; Doktorov, A. B. *J. Chem. Phys.* **1996**, *105*, 2320.
(23) Gopich, I. V.; Kipriyanov, A. A.; Doktorov, A. B. *J. Chem. Phys.* **1999**, *110*, 10888.
(24) Popov, A. V.; Agmon, N. *J. Chem. Phys.* **2001**, *115*, 8921.
(25) Popov, A. V.; Agmon, N. *J. Chem. Phys.* **2002**, *117*, 4376.
(26) Popov, A. V.; Agmon, N. *J. Chem. Phys.* **2003**, *118*, 11057.
(27) Agmon, N.; Popov, A. V. *J. Chem. Phys.* **2003**, *119*, 6680.
(28) Park, S.; Shin, K. J.; Popov, A. V.; Agmon, N. *J. Chem. Phys.* **2005**, *123*, 034507.
(29) Zhou, H.-X. *J. Phys. Chem. B* **1997**, *101*, 6642.
(30) Kim, H.; Yang, M.; Choi, M.-U.; Shin, K. J. *J. Chem. Phys.* **2001**, *115*, 1455.
(31) Park, S.; Agmon, N. *J. Phys. Chem. B* **2008**, *112*, 5977.
(32) Rice, S. A. *Diffusion-Limited Reactions*. Comprehensive Chemical Kinetics Series; Elsevier: Amsterdam, 1985; Vol. 25.
(33) Andre, J. C.; Baros, F.; Winnik, M. A. *J. Phys. Chem.* **1990**, *94*, 2942.
(34) Agmon, N. *Phys. Rev. E* **1993**, *47*, 2415.
(35) Edelstein, A. L.; Agmon, N. *J. Chem. Phys.* **1993**, *99*, 5396.
(36) Gopich, I. V.; Agmon, N. *J. Chem. Phys.* **1999**, *110*, 10433.
(37) Park, S. H.; Peng, H.; Kopelman, R.; Argyrakis, P.; Taitelbaum, H. *Phys. Rev. E* **2006**, *73*, 041104.

JP803873P